Shap. Mem. Superelasticity (2017) 3:250–263
DOI 10.1007/s40830-017-0115-2

Fatigue Modeling for Superelastic NiTi Considering Cyclic Deformation and Load Ratio Effects

Mohammad J. Mahtabi[1,2] · Nima Shamsaei[3]

Published online: 3 August 2017

Abstract A cumulative energy-based damage model, called total fatigue toughness, is proposed for fatigue life prediction of superelastic NiTi alloys with various deformation responses (i.e., transformation stresses), which also accounts for the effects of mean strain and stress. Mechanical response of superelastic NiTi is highly sensitive to chemical composition, material processing, as well as operating temperature; therefore, significantly different deformation responses may be obtained for seemingly identical NiTi specimens. In this paper, a fatigue damage parameter is proposed that can be used for fatigue life prediction of superelastic NiTi alloys with different mechanical properties such as loading and unloading transformation stresses, modulus of elasticity, and austenite-to-martensite start and finish strains. Moreover, the model is capable of capturing the effects of tensile mean strain and stress on the fatigue behavior. Fatigue life predictions using the proposed damage parameter for specimens with different cyclic stress responses, tested at various strain ratios ($R_\varepsilon = \varepsilon_{min}/\varepsilon_{max}$) are shown to be in very good agreement with the experimentally observed fatigue lives.

Keywords Fatigue · Mean stress · Energy method · Nitinol · Life prediction · Superelasticity · Shape memory alloy

List of Symbols

$2N_f$	Number of reversals to failure
A → M	Austenite-to-martensite transformation
E_A	Austenite modulus of elasticity
M → A	Martensite-to-austenite transformation
N_f	Experimental number of cycles to failure
$N_{f,p}$	Predicted number of cycles to failure
R_ε	Strain ratio in a cyclic loading ($\varepsilon_{min}/\varepsilon_{max}$)
W_d	Dissipated strain-energy-density
W_e^+	Tensile austenitic strain-energy-density
W_t	Total strain-energy-density
ε_a	Strain amplitude (i.e., alternating strain)
ε_m	Mean strain
ε_{max}	Maximum strain
ε_{min}	Minimum strain
ε_f^{AM}	A → M finish strain
ε_f^{MA}	M → A finish strain
ε_s^{AM}	A → M start strain
σ_a	Stress amplitude (i.e., alternating stress)
σ_m	Mean stress
σ_{max}	Maximum stress
σ_{min}	Minimum stress
σ_f^{MA}	M → A finish stress (i.e., unloading transformation stress)
σ_s^{AM}	A → M start stress (i.e., loading transformation stress)
ΣW_d	Cumulative dissipated strain-energy-density
ΣW_t	Total fatigue toughness (cumulative total strain-energy-density)

✉ Nima Shamsaei
shamsaei@auburn.edu

[1] Department of Mechanical Engineering, Mississippi State University, Mississippi State, MS 39762, USA

[2] Center for Advanced Vehicular Systems (CAVS), Mississippi State University, Mississippi State, MS 39762, USA

[3] Laboratory for Fatigue & Additive Manufacturing Excellence (FAME), Department of Mechanical Engineering, Auburn University, Auburn, AL 36849, USA

Introduction

Fatigue analysis has become a critical part of designing components made of NiTi, an almost equiatomic alloy of nickel and titanium, as they are often under cyclic service loads. For instance, self-expanding stents made of NiTi are under a cyclic load caused by the heartbeat, in addition to the constant load/deformation applied by the peripheral vessel [1]. Furthermore, in many other structural applications such as in bridges, NiTi elements are under cyclic loading, coming from various dynamic external loads such as moving vehicles, wind, and earthquake [2]. NiTi has been employed for several applications in various industries such as biomedical [3, 4], aerospace and automotive [5], for which a reliable fatigue-resistant component design is very important. Consequently, extensive research projects have been recently conducted to investigate the fatigue behavior of this alloy [6–8]. Moreover, several attempts have been made to analyze and model the fatigue behavior of superelastic NiTi in the low-cycle fatigue regime by means of a modified Coffin–Manson approach (e.g., [9, 10]).

While NiTi wire specimens under rotating bending test setup have been mostly used to characterize the fatigue performance of this shape memory alloy (e.g., [11–13]), there are only a handful of studies (e.g., [14, 15]) that have employed larger cylindrical specimens. Specimens in these studies were circular with uniform gage section and were subjected to uniaxial cyclic loading. Very limited studies can be found on the experimental and modeling aspects of more complex, yet realistic, types of loading such as torsion [16] and multiaxial loading [17, 18]. Mean strains/stresses also often exist in real-time applications of NiTi components such as stents [19]; therefore, it is critical to study and model their fatigue behaviors under non-zero mean strains/stresses.

Mahtabi and Shamsaei [20] recently evaluated the applicability of well-known mean stress fatigue models and illustrated that the classical fatigue models do not work appropriately for superelastic NiTi. This is mainly resulting from the NiTi's unique stress–strain response, driven by the forward and backward austenite-to-martensite (A $\leftrightarrow$ M) phase transformations in this material. In addition to the unique mechanical response of NiTi, fatigue resistance of superelastic NiTi is shown to be highly sensitive to tensile mean stress [15, 18, 20, 21], which makes fatigue modeling of this material even more challenging. They [20] proposed an energy-based damage parameter based on the Ellyin and coworkers' approach [22, 23] that considers the effect of tensile austenitic strain-energy-density on the fatigue damage. Their proposed damage parameter, calculated based on the stable cycle of the stress–strain response of the material, correlated well with the experimental fatigue lives of the superelastic NiTi with various strain ratios ($R_\varepsilon = \varepsilon_{min}/\varepsilon_{max}$). However, the data used in their study [20] only included a number of experiments that had similar stress response (i.e., comparable transformation stresses).

The mechanical response of NiTi is highly sensitive to the chemical composition [24] and manufacturing and postmanufacturing [25–27] processing, which influence the microstructural properties such as grain size, precipitation, texture, and characteristic temperatures. The material response is also dependent on the testing/operating conditions such as temperature and strain rate [28]. Therefore, significantly different transformation stresses (i.e., deformation response) may be obtained for NiTi because of a small difference in transformation temperatures and/or the operating temperature [26, 29–31]. Due to these effects, conducting a series of fatigue experiments on different specimens may result in different deformation responses, making the fatigue analysis of this alloy very challenging. The main objective of this study is to propose a unified damage model that can correlate the fatigue behavior of superelastic NiTi with various mechanical properties such as loading and unloading transformation stresses, austenite-to-martensite transformation (A $\rightarrow$ M) start strain, and modulus of elasticity. The model will also be able to consider the effects of mean stress/strain on the fatigue behavior of superelastic NiTi.

Background

Morrow and Halford [32, 33] showed that the required amount of energy to cause fatigue failure in the material increases as the number of cycles of loading to failure increases. Halford [32] collected a large number of fatigue data for different materials and reported a linear relationship between what they called "Fatigue Toughness" (calculated as the sum of the dissipated strain-energy densities of all the cycles to failure) of materials and the number of cycles to failure in a log–log plot. The linear equation in the log–log scale had a positive slope indicating an increasing amount of energy for larger number of cycles to failure (i.e., smaller amount of cyclic load). The portion of energy considered in Halford's study was equal to the sum of the hysteresis energy of the material, equivalent to the area encompassed by loading and unloading paths (i.e., the dissipated strain-energy-density, W_d), for all the cycles to failure.

Nip et al. [34] also used Halford's cumulative dissipated strain-energy-density approach for axial and bending tests on three different types of steel and concluded that the cumulative total dissipated energy is a suitable damage

parameter for predicting the fatigue failure. The cumulative dissipated strain-energy-density (plastic strain-energy-density) has been also used to analyze the fatigue behavior of metallic and polymeric materials by other researchers [35–37].

The main issue of employing a fatigue damage parameter based on W_d is the fact that it yields a zero value in the linear elastic region, where the loading and unloading paths on a stress–strain response of the material overlay. However, fatigue failures have been reported for superelastic NiTi [12] within the linear elastic region. Moreover, for majority of the materials, mean stress effects are more pronounced when deformation is fully elastic, probably due to lower mean stress relaxation. Therefore, a fatigue damage parameter based on W_d may not appropriately account for the effects of mean stress/strain in the linear elastic region.

Furthermore, for common metals, the movement of the dislocations, resulting in plastic strain, and the corresponding resistance to this movement (i.e., cyclic stress response), are the two main phenomena that dissipate the mechanical energy and form the hysteresis loop [33]. For superelastic NiTi, however, a different mechanism is causing the formation of the hysteresis loop and that is the transformation of the material between austenite (B2 structure) and martensite (B19′ structure) phases during loading and unloading. As a result, the dissipated strain-energy-density may only represent the contribution of the phase transformation to damage. Therefore, more terms such as tensile austenitic strain-energy-density, W_e^+, [20, 23], may be needed to consider other mechanisms contributing to the overall fatigue damage in the material.

Material and Experiments

The material used in this study was $Ni_{50.8}Ti_{49.2}$ (at.%), obtained in the form of straight circular bars of 10 mm diameter. The straight bars were machined to cylindrical fatigue specimens with uniform gage section of ~7 mm diameter and 17 mm length. Compared with common metallic materials, superelastic NiTi typically exhibits significantly longer fatigue life at a certain strain level. For instance, while common metallic materials do not last more than ~2000 cycles under 1% fully reversed cyclic straining, superelastic NiTi typically exhibits a fatigue life longer than 65,000 cycles [14]. Consequently, it is possible to run fatigue tests on NiTi specimens at relatively large strain levels, compared with other metallic materials. For fully-reversed tests at large strain levels, buckling of the specimen can be the main challenge. In order to overcome this issue, the diameter of the gage section was selected large enough to minimize the possibility of buckling for fully reversed tests at larger values of strain amplitude (e.g., 1.5%).

Heat treatment was conducted after machining the specimens to eliminate any possible undesired effects of machining on the residual phase transformation in the material and to obtain austenitic NiTi specimens. The heat treatment included a short annealing in salt bath (for ~2 min) at 550 °C, followed by quenching in iced water. Heat-treated specimens were then mechanically polished using sand papers up to grit #4000, to provide a very smooth surface finish and minimize the effects of surface flaws on the fatigue behavior. Since mechanical properties of NiTi, such as modulus of elasticity, loading, and unloading transformation stresses, and A → M start strain are very sensitive to the heat treatment and processing, NiTi specimens with various mechanical properties were obtained even by a slight change in the duration of the annealing time.

Details of experimentations were similar to the authors' previous works [14, 20]. Cyclic tests were conducted in strain-controlled condition using an MTS servohydraulic fatigue machine at room temperature (~24 °C). Measuring the strain was made using an MTS uniaxial extensometer with a gage length of 15 mm. The average strain rate of all cyclic tests was held constant; thus, the frequency of each test was adjusted depending on the applied strain amplitude. The surface temperature of some specimens was measured using a laser thermometer, and no significant temperature increase was observed during fatigue testing. The range of variations in surface temperature of the specimens was within 1 °C. Cyclic tests were conducted at various strain ratios such as fully-reversed ($R_\varepsilon = -1$), pulsating ($R_\varepsilon = 0$), and tension–tension ($R_\varepsilon > 0$) using a sinusoidal waveform. The tension–tension tests included a set of data at $R_\varepsilon = 0.5$ and some other tests that were designed based on various combinations of mean strain and strain amplitude. Thus, various strain ratios were considered for the tests in the latter condition, which are referred to here as $R_\varepsilon = VAR$.

Experimental Results

As mentioned earlier, the mechanical properties of NiTi are highly dependent to the processing factors and a slight change in the operating/testing temperature and/or chemical composition of NiTi can alter these properties significantly. Among the different mechanical properties, loading and unloading transformation stresses are the ones most influenced by the processing. In this study, a wide range of mechanical properties was obtained for different specimens, tested at room temperature.

Figure 1 illustrates the stress–strain response of two selected specimens, tested in this study, demonstrating the wide range of the mechanical behavior obtained for these specimens. Both specimens in Fig. 1a, b were tested in strain-controlled pulsating condition ($R_\varepsilon = 0$) and up to a maximum strain of 2.0%. As seen, the specimen with higher stress response (i.e., Fig. 1a) had an A → M start strain of 1.1% and a corresponding stress equal to 562 MPa. The corresponding strain and stress values for the end of the reverse transformation (martensite-to-austenite transformation, M → A) were $\varepsilon_f^{MA} = 0.9\%$ and $\sigma_f^{MA} = 489$ MPa. On the other hand, the specimen with lower transformation stress (i.e., Fig. 1b) had an A → M start strain and stress values of 0.9% and 477 MPa, respectively. M → A transformation was finished at $\varepsilon_f^{MA} = 0.8\%$ and $\sigma_f^{MA} = 409$ MPa during unloading, as seen in Fig. 1b. It is worth mentioning that the commonly used 0.2% offset for identifying the yield point in metallic material was employed here to determine the stress and strain values corresponding to the phase transformation limits.

Although both specimens in Fig. 1 exhibit similar modulus of elasticity in the linear elastic region, this is not the case for all the specimens in this study. Table 1 lists the different deformation properties of the specimens tested in this study. As can be seen in Table 1, there is a significant variation in the modulus of elasticity of different specimens. Specimens in this study exhibited a wide range of mechanical properties: such as loading transformation stress ($\sigma_s^{AM} = 350$–560 MPa), A → M start strain ($\varepsilon_s^{AM} = 0.7$ – 1.4%), and austenite modulus of elasticity ($E_A = 45$–80 GPa).

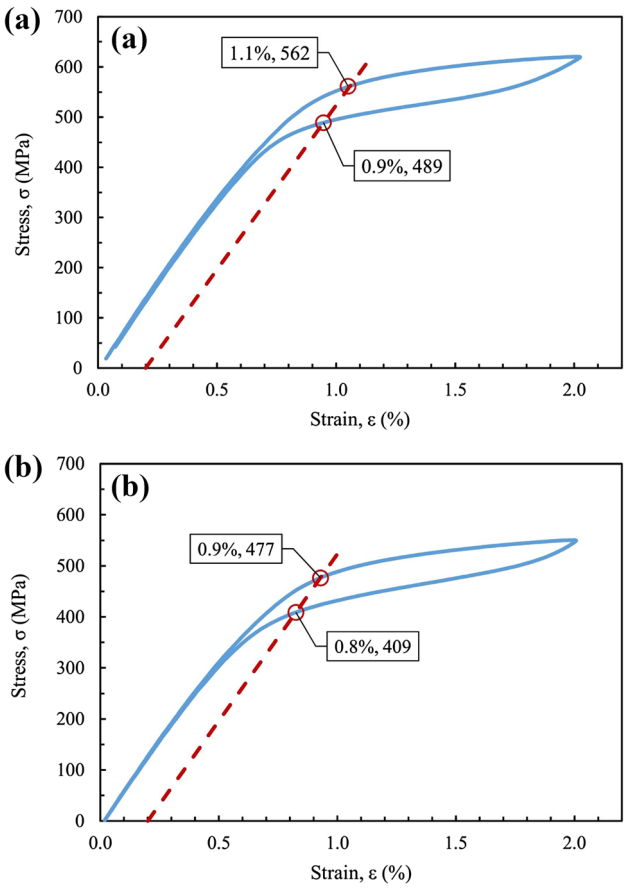

Fig. 1 First-cycle stress–strain responses of selected specimens used in this study indicating a wide range of mechanical properties: **a** high transformation stress and **b** low transformation stress

Experimental results from fatigue tests are listed in Table 2, which includes strain amplitude, mean strain, stress amplitude and mean stress, as well as the different strain-energy-densities associated with the cyclic response of the material. The reported values for the stress amplitude and mean stress as well as the strain-energy-densities in this table belong to the stable cycle of the material response, recorded near the midlife of each specimen. Some of the data at fully-reversed, pulsating, and $R_\varepsilon = 0.5$ in this study are taken from authors' previous work [20]. Fatigue life observations for various specimens, tested at different strain ratios and strain amplitudes are shown in Fig. 2. $R_\varepsilon =$ VAR in this figure indicates strain ratios other than −1, 0, and 0.5. The actual value of R_ε for these experiments are listed in Table 2.

Figure 2a illustrates the strain-life data categorized based on the strain ratio, and Fig. 2b groups the same data based on the level of the loading transformation stress (i.e., σ_s^{AM}). As seen in these figures, a wide scatter exists in the fatigue data at different strain levels. Strain-life plot of Fig. 2a indicates a significant reduction in the fatigue life of the superelastic NiTi in the presence of tensile mean stress/strain [20]. Similar to common metals, this effect is more pronounced in longer fatigue life regime as can be noticed by comparing the data at $\varepsilon_a \leq 1.0\%$ in this figure.

Stress amplitudes of all fatigue experiments, reported in Table 2, are plotted against fatigue lives shown in Fig. 3a, b, indexed based on the strain ratio and the level of the loading transformation stress (i.e., σ_s^{AM}), respectively. As mentioned earlier, the stress values are obtained from the stable cycle of the material response. Similar to the strain-life analysis, the specimens tested in fully-reversed condition exhibited significantly longer fatigue lives compared with the non-zero mean strain/stress tests, indicating severe detrimental effects of tensile mean strain/stress on fatigue resistance of this material.

Fatigue Modeling

Fatigue analysis and modeling of the superelastic NiTi specimens with different mechanical properties such as modulus of elasticity, loading/unloading transformation stress, and A → M start strain are discussed in this

Table 1 Deformation properties of NiTi specimens used in this study

Test	E_A (MPa)	ε_s^{AM} (%)	ε_f^{MA} (%)	σ_s^{AM} (MPa)	σ_f^{MA} (MPa)
1	67,578	0.94	0.87	503	454
2	69,344	0.90	0.80	473	419
3	71,806	0.92	0.87	519	480
4	65,105	0.90	0.80	448	405
5	65,325	0.95	0.90	484	449
6	64,934	1.00	0.95	550	493
7	61,380	0.91	0.85	433	397
8	69,860	0.70	0.60	363	307
9	65,960	0.95	0.92	496	476
10	70,394	0.85	0.80	455	420
11	50,200	1.20	1.00	510	423
12	57,195	1.15	1.01	545	466
13	67,498	0.94	0.75	500	372
14	66,567	1.06	0.95	562	489
15	52,716	1.00	0.80	434	312
16	57,300	1.10	0.90	491	410
17	66,254	0.90	0.80	488	417
18	65,387	0.93	0.83	477	409
19	67,462	0.90	0.80	494	424
20	67,450	0.90	0.80	459	406
21	67,206	1.03	0.93	558	494
22	67,411	1.02	0.94	554	496
23	66,408	1.02	0.94	546	490
24	70,426	0.90	0.80	487	448
25	68,649	0.72	0.63	359	298
26	61,200	1.10	–	520	–
27	66,693	0.75	0.67	364	316
28	73,416	0.90	0.80	515	429
29	79,100	0.90	0.75	515	433
30	71,595	0.90	0.80	503	460
31	73,113	0.90	0.80	500	447
32	50,159	1.20	1.10	517	453
33	79,360	0.80	0.75	498	459
34	74,918	0.70	0.55	356	260
35	69,735	0.88	0.82	474	430
36	72,663	0.90	0.85	509	470
37	69,976	0.92	0.87	502	460
38	67,485	0.72	0.60	349	270
39	63,910	0.99	0.90	503	445
40	80,334	0.84	0.73	516	425
41	68,696	0.73	0.61	366	282
42	68,767	0.91	0.81	486	425
43	57,828	0.98	0.83	449	360
44	45,537	1.43	1.23	560	470
45	48,920	1.34	1.10	558	438

section. Considering the fact that fatigue models based on only stress or strain are not appropriate candidates for analyzing the fatigue behavior of superelastic NiTi [20], energy-based models have been used in this study. Energy-based fatigue models reflect the shape of the stress–strain response of the material, and therefore, they consider the effects of both stress and strain terms on the fatigue behavior [15, 20]. In the following sections, fatigue behavior of superelastic NiTi is studied by considering various components of energy, associated with the stress–strain response of the material, such as dissipated (W_d) and tensile elastic (W_e^+) energy densities. An attempt has been made here to develop an energy-based fatigue damage parameter, which can correlate the fatigue data for superelastic NiTi from specimens with different mechanical properties, as shown in Fig. 1.

Dissipated Strain-Energy-Density

The dissipated strain-energy-density, W_d, is equal to the area encompassed by loading and unloading paths on the stress–strain responses of the material in one cycle of loading, typically a cycle near the mid-fatigue life of the specimen [20]. For fully-reversed tests, the stress–strain response of the superelastic NiTi exhibits two different segments in tension and compression. First-cycle and stable-cycle stress–strain responses of two tests under fully-reversed condition are shown in Fig. 4. As can be seen in this figure, superelastic NiTi exhibits a large asymmetry in tension and compression with the loading transformation stress in compression being significantly larger than that in tension. Accordingly, both segments were considered in calculating the dissipated strain-energy-density, W_d. It should be noted that as the loading transformation stress under compression is larger than that in tension (due to asymmetry in tension and compression), under strain-controlled loading, the compressive transformation strain (i.e., amount of strain beyond the linear elastic regime) is different from the tensile one. The different values of transformation strains result in different sizes of hysteresis loops in tension and compression. Thus, the effect of tension–compression asymmetry is inherently accounted for when both tensile and compressive dissipated strain-energy-densities (i.e., W_d) are included in the damage parameter. In order to calculate W_d, a subroutine was developed to calculate the area of the stress–strain curve using the values of stress and strain obtained from midlife cyclic data.

Figure 5 exhibits the dissipated strain-energy-density, as the damage parameter, against the experimentally observed fatigue lives for different tests, listed in Table 2. As seen in this figure, there is a large scatter between different tests at

Table 2 Details of fatigue experiments and analysis results for the investigated NiTi specimens

Test	$2N_f$	R_ε	ε_a (%)	ε_m (%)	σ_a (MPa)	σ_m (MPa)	W_d (MJ/m^3)	W_t (MJ/m^3)	ΣW_d (MJ/m^3)	ΣW_t (MJ/m^3)
1[a]	5170	−1	1.50	0.00	625	−73	0.46	2.72	1214	7053
2	6076		1.50	0.00	677	−131	0.52	2.67	1695	8363
3	8412		1.50	0.00	721	−109	0.49	3.09	2058	13,021
4[a]	11,906		1.25	0.00	602	−89	0.39	2.42	2334	14,348
5[a]	15,116		1.10	0.00	597	−69	0.25	2.38	1941	17,900
6	20,992		1.25	0.00	693	−114	0.24	2.82	1419	27,305
7	72,642		1.10	0.00	535	−122	0.33	1.72	12,540	60,680
8	119,396		1.00	0.00	495	−56	0.32	1.70	19,789	101,987
9	>68,726		1.00	0.00	602	−119	0.23	1.99	7286	69,190
10[a]	>134,878		1.00	0.00	582	−156	0.08	1.37	6146	93,995
11	1276	0	1.50	1.50	284	304	1.32	4.77	850	3039
12	1300		1.50	1.50	387	284	1.17	5.10	771	3313
13	1612		1.50	1.50	455	231	1.17	4.66	1011	3785
14	2888		1.00	1.00	338	321	0.54	3.81	801	5486
15[a]	2974		1.50	1.50	434	126	1.04	4.02	1636	6099
16[a]	2978		1.50	1.50	405	167	1.76	4.61	2609	6846
17[a]	3542		1.00	1.00	371	192	0.40	2.80	743	4987
18	3662		1.00	1.00	304	269	0.50	3.01	942	5524
19[a]	4666		1.00	1.00	346	223	0.34	2.74	744	6394
20	4920		1.00	1.00	278	278	0.49	2.78	1234	6827
21	5836		1.00	1.00	355	297	0.48	3.64	1436	10,648
22	18,912		0.70	0.70	305	311	0.21	3.02	2026	28,536
23	19,356		0.70	0.70	310	293	0.20	2.94	1934	28,428
24[a]	23,212		0.50	0.50	256	249	0.09	1.90	1046	22,065
25	>210,580		0.50	0.50	245	169	0.12	1.36	12,193	144,169
26	>216,410		0.50	0.50	251	260	0.03	2.17	3450	234,007
27	>721,204		0.45	0.45	212	199	0.11	1.38	39,948	497,830
28[a]	2716	0.5	1.00	3.00	199	451	0.28	3.16	431	4373
29[a]	3066		1.00	3.00	179	464	0.47	3.08	759	4771
30[a]	8152		0.50	1.50	87	478	0.18	2.41	769	9834
31[a]	9094		0.40	1.20	66	476	0.16	2.17	725	9926
32	11,054		0.50	1.50	69	455	0.29	3.03	1575	16,824
33[a]	12,426		0.40	1.20	66	472	0.13	1.95	808	12,216
34	130,626		0.40	1.20	118	316	0.10	1.36	6173	87,549
35	16,638	VAR	0.40	0.80	110	413	0.15	2.10	1214	17,361
36	24,692		0.40	0.80	146	392	0.09	2.08	1143	25,694
37	9422		0.50	2.00	82	472	0.21	2.40	992	11,282
38	35,866		0.50	2.00	148	277	0.15	1.49	2705	26,623
39	9066		0.50	2.50	86	456	0.21	2.51	960	11,411
40	10,740		0.50	2.50	100	456	0.14	2.06	781	11,229
41	99,016		0.40	2.20	123	288	0.10	1.33	4779	65,699
42	21,294		0.30	2.20	60	448	0.09	1.97	985	21,052
43	138,458		0.20	3.80	59	362	0.03	1.56	1922	107,784
44	255,066		0.20	3.80	56	457	0.01	2.90	1792	369,165
45	259,594		0.20	3.80	48	488	0.02	2.96	2023	380,911

[a] Data from Mahtabi and Shamsaei [20]

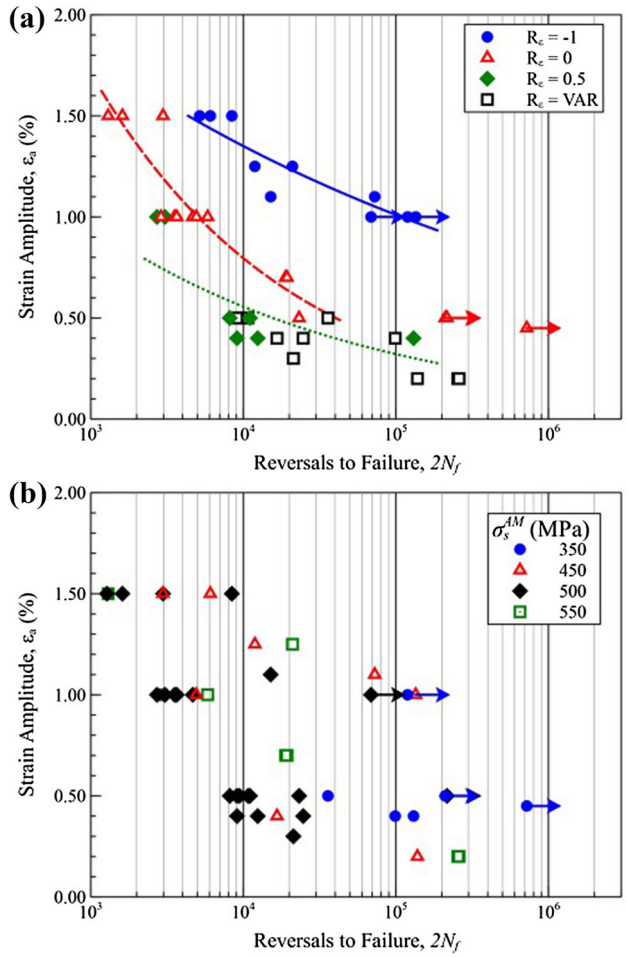

Fig. 2 Strain-life fatigue data for superelastic NiTi with different mechanical properties tested at different strain ratios (R_ε), categorized based on **a** R_ε, and **b** σ_s^{AM}. *Arrows* indicate failure in the grip

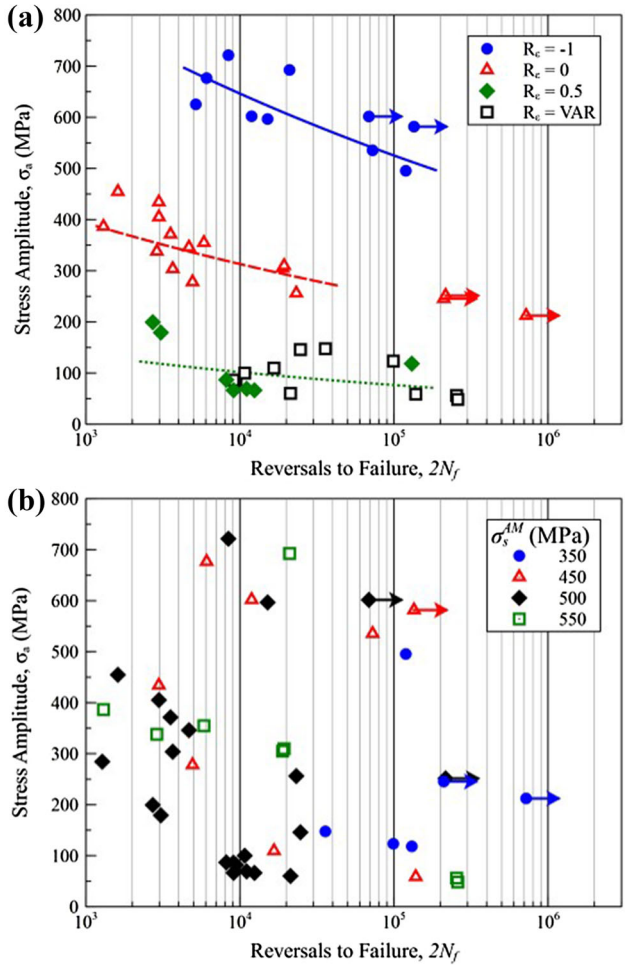

Fig. 3 Stress-life fatigue data for superelastic NiTi with different mechanical properties tested at different strain ratios (R_ε), categorized based on **a** R_ε, and **b** σ_s^{AM}. *Arrows* indicate failure in the grip

a certain W_d. Therefore, the dissipated strain-energy-density, W_d, may not be an appropriate damage parameter to correlate data from various testing conditions and specimens with different cyclic deformation responses.

Cumulative Disspated Strain-Energy-Density

As previously discussed, Halford and Morrow [32, 33] observed that the cumulative area of the cyclic hysteresis loop of material, ΣW_d, can be considered as an indicator of the fatigue damage. They calculated and reported the cumulative dissipated strain-energy-density for several materials such as steels, titanium, and aluminum alloys, in one plot, and the results from their calculations illustrated a reasonable correlation between the fatigue life and the amount of ΣW_d. The same concept is examined here to correlate the fatigue data of superelastic NiTi with different mechanical responses and under different loading conditions. The cumulative dissipated strain-energy-density in this study is calculated by adding the dissipative strain-energy-density of every cycle of loading until failure, as expressed by Eq. (1). For cases where there was a gap between two recorded cycles, an interpolation was made to calculate the cumulative strain-energy-density for unrecorded cycles.

$$\Sigma W_d = \sum_{i=1}^{N_f} (W_d)_i. \quad (1)$$

Figure 6 presents the cumulative dissipated strain-energy-density values, ΣW_d, for different NiTi specimens and test conditions against the experimentally observed fatigue lives. The tests are categorized based on the loading condition in Fig. 6a, while in Fig. 6b, the mechanical properties were the basis of classification. As can be seen in these figures, the correlation between the experimental data and the damage parameter is not promising for the data under different loading conditions and with different deformation responses. Moreover, the scatter in the fatigue lives of the specimens, at the same level of cumulative dissipated strain-energy-

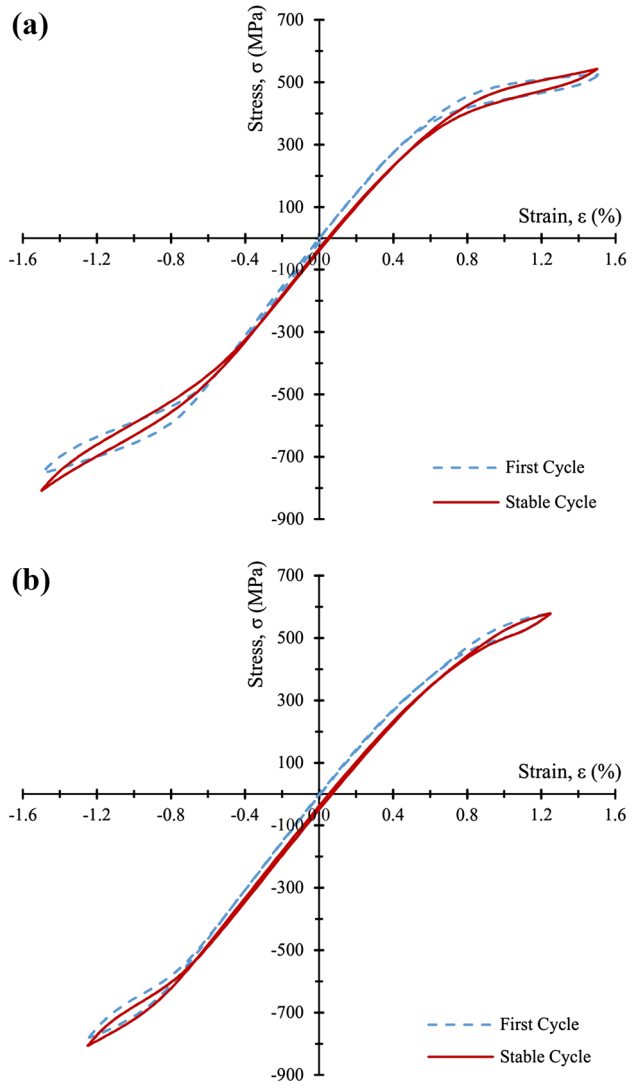

Fig. 4 First-cycle and stable-cycle stress–strain responses of two tests under fully reversed condition: **a** $\varepsilon_a = 1.5\%$ and **b** $\varepsilon_a = 1.25\%$

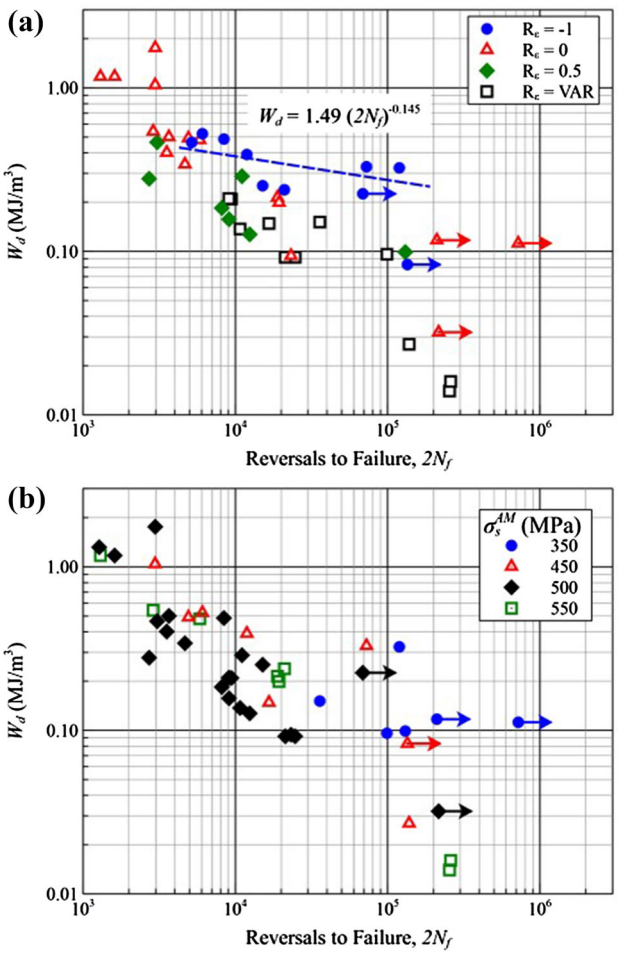

Fig. 5 Dissipated strain-energy-density, W_d, versus fatigue life for different tests categorized based on **a** R_ε, and **b** σ_s^{AM}. *Arrows* indicate failure in the grip

denisty, is large. This scatter will result in inaccurate fatigue life predictions, as will be discussed later in this paper.

Total Strain-Energy-Density

Mahtabi and Shamsaei [20] proposed an energy-based damage parameter based on the works by Ellyin and coworkers [22, 23], which considers the effect of both dissipated and tensile austenitic strain-energy-densities. Illustration of the different strain-energy-densities considered in their model is shown in Fig. 7. According to this figure, the total strain-energy-density, as the indicator of the fatigue damage, can be calculated using the following equation:

$$W_t = W_d + W_e^+, \tag{2}$$

where W_d, the dissipated strain-energy-density, is the same as what was explained before. W_e^+, tensile austenitic strain-energy-density, is an energy term, which considers the effect of maximum tensile stress on the fatigue resistance of superelastic NiTi. The term "tensile austenitic strain-energy-density" should not be confused with the elastic strain-energy-density in the material, which is related to the effective elastic modulus of the partially or fully transformed material [10]. W_e^+ is defined as the area of the triangle generated by a hypothetical linear elastic unloading of the material and can be calculated based on the maximum stress, σ_{max}, and austenite modulus of elasticity, E_A, using the following equation [20]:

$$W_e^+ = \frac{\sigma_{max}^2}{2E_A}. \tag{3}$$

Since, in a cyclic loading, maximum stress is equal to the sum of the mean stress, σ_m, and the stress amplitude, σ_a, the tensile elastic strain-energy-density can also be written in the form of Eq. (4), indicating the capability of this model to account for the effect of mean stress on fatigue resistance.

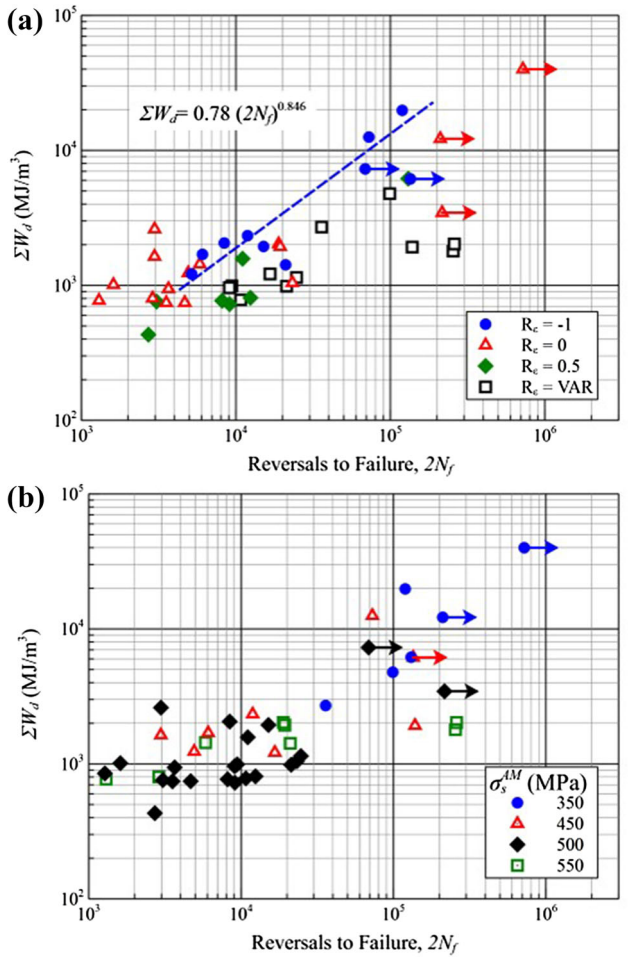

Fig. 6 Cumulative dissipated strain-energy-density, ΣW_d, versus life for different tests categorized based on **a** R_ε, and **b** σ_s^{AM}. *Arrows* indicate failure in the grip

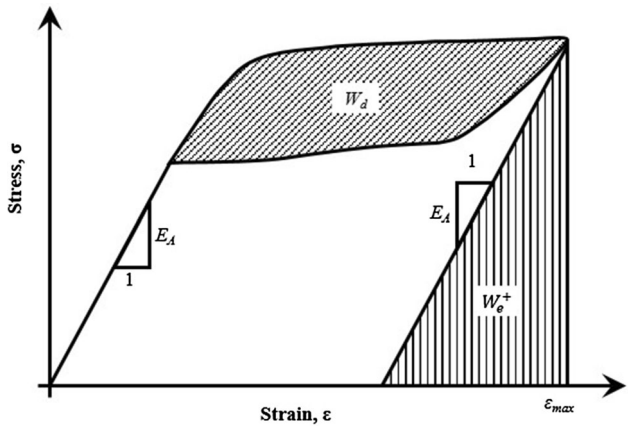

Fig. 7 Schematic showing the energy terms associated with the total strain-energy-density damage parameter [20] for superelastic NiTi

$$W_e^+ = \frac{(\sigma_a + \sigma_m)^2}{2E_A}. \quad (4)$$

It is worth mentioning that the term "total," used for naming this damage parameter, does not mean that the whole area under the stress–strain curve (referred to as tensile superelastic strain-energy-density in [20]) should be considered for W_e^+. In fact, only the tensile austenitic strain-energy-density, as illustrated in Fig. 7, should be considered for the W_e^+ term in Eq. (2). For specimens under fully reversed condition ($R_\varepsilon = -1$), the dissipated strain-energy-density values in both compression and tension sides of the stress–strain curve, as seen in Fig. 4, should be included in the damage calculation. Moreover, the tensile austenitic strain-energy-density, W_e^+, should be only calculated for the tensile part of the stress–strain response. Similar to the calculations for the dissipated strain-energy-density, the effects of tension–compression asymmetry in the material response is accounted for in the W_d part of the total strain-energy-density. It is shown that the fatigue life predictions using W_t damage parameter yielded acceptable results for superelastic NiTi specimens with similar deformation response, but under various mean strain loadings [20]. Although they reported satisfactory results using either the first cycle or the stable cycle of deformation response to calculate the energy terms, they recommended the use of stable cycle, since it considers the various aspects of cyclic loading, including; cyclic hardening/softening, mean stress relaxation, and the evolution of the hysteresis loop under cyclic loading. Thus, the damage parameter used in this section is calculated based on the stable response of the material.

Figure 8 presents the total strain-energy-density, W_t, plotted against the experimental fatigue lives for all superelastic NiTi data in this study. As seen in Fig. 8a, not an acceptable correlation is obtained between the experimental data at different strain ratios. Figure 8b shows the same data grouped based on the level of loading transformation stress (i.e., σ_s^{AM}) of the material. As seen in this figure, unlike the models previously discussed, the data related to the specimens with comparable transformation stresses follow a linear trend in the log–log plot, and somewhat less scatter is observed for each set of experiments having a similar transformation stress, but tested at different strain ratios. This may indicate that although their proposed energy model appropriately accounts for the effects of mean stress/strain on the fatigue behavior of superelastic NiTi, as reported in [20], its applicability may be limited to the test specimens with comparable transformation stresses (i.e., cyclic deformation response).

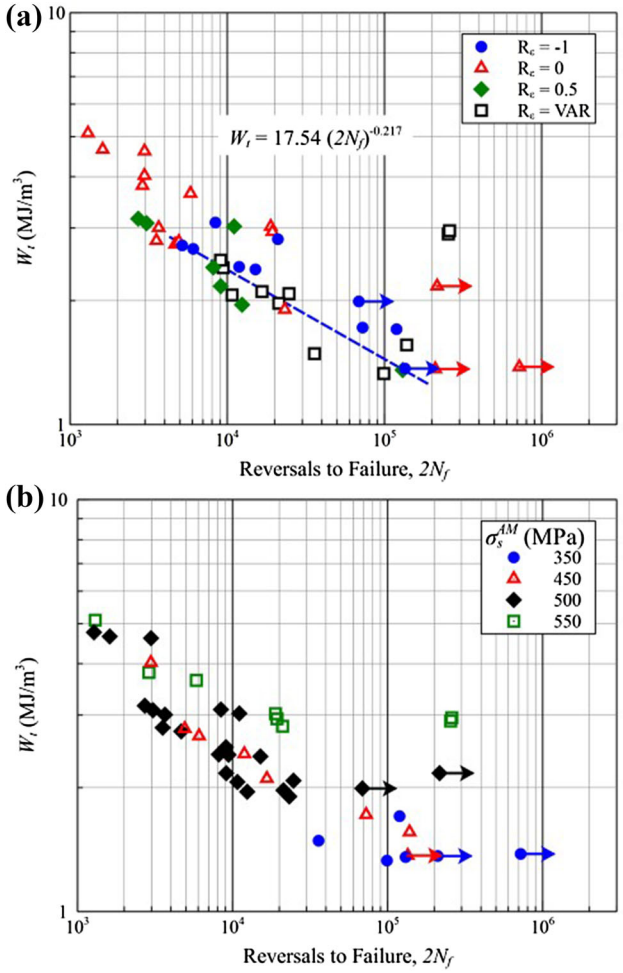

Fig. 8 Total strain-energy-density, W_t, versus fatigue life for different tests categorized based on **a** R_ε, and **b** σ_s^{AM}. *Arrows* indicate failure in the grip

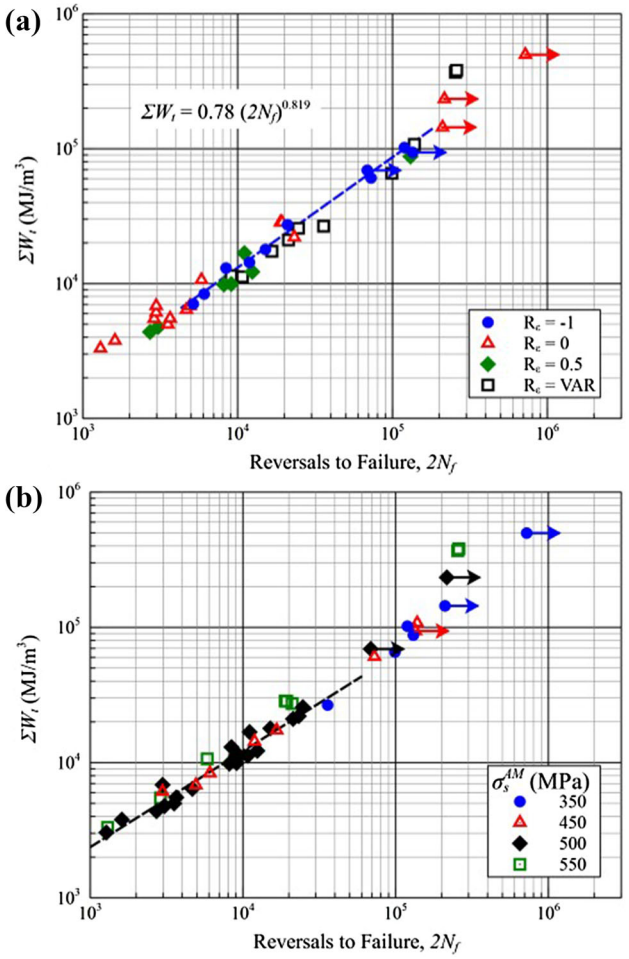

Fig. 9 Cumulative total strain-energy-density, ΣW_t, versus fatigue life for different tests categorized based on **a** R_ε, and **b** σ_s^{AM}. *Arrows* indicate failure in the grip

Total Fatigue Toughness

The concept of cumulative dissipated strain-energy-density under cyclic loading is extended to the fatigue analysis of superelastic NiTi in this study based on the total strain-energy-density damage parameter, previously proposed by Mahtabi and Shamsaei [20], and is called total fatigue toughness, following the notation by Halford and Morrow [32, 33]. The total fatigue toughness, ΣW_t, which is proposed here as the damage parameter, is defined as the summation of the total strain-energy-density at each loading cycle and can be calculated as

$$\Sigma W_t = \sum_{i=1}^{N_f} (W_t)_i = \sum_{i=1}^{N_f} \left(W_d + W_e^+\right)_i. \quad (5)$$

The total fatigue toughness, ΣW_t, is plotted against the experimental fatigue lives of superelastic NiTi specimens shown in Fig. 9a, b, categorized based on the applied strain ratio, R_ε, and the transformation stress of the material, σ_s^{AM}, respectively. As seen in these figures, a linear relationship, in a log–log scale, can represent the fatigue behaviors of the tests from different conditions. This means that the proposed damage parameter in this study very well correlates with the fatigue data from different transformation stresses and tested at different strain ratios. It should be mentioned that similar to the cumulative dissipated strain-energy-density, an interpolation was made to account for the total strain-energy-densities of unrecorded cycles.

The close correlation between the data from various material deformation responses (i.e., transformation stresses) and testing conditions illustrates the capability of the total fatigue toughness as the damage parameter for fatigue life prediction of superelastic NiTi. Therefore, one single equation can be used for fatigue life prediction of superelastic NiTi specimens with different deformation responses, as long as the material exhibits superelastic behavior.

Discussions

Fatigue life predictions using the different energy-based damage parameters, explained in the previous section, are provided in Fig. 10 in comparison to the experimentally observed fatigue lives. The data in this figure are categorized based on the applied strain ratio. In Fig. 10, a vertical arrow indicates an infinite predicted fatigue life, and a 45° angle arrow stands for both experimental and predicted fatigue lives being infinite (i.e., runout). It is also worth mentioning that the fatigue life prediction using the cumulative strain-energy-densities for specimens that failed in the grip was done based on the deformation responses up to the applied number of cycle since the actual fatigue life of the specimen was unknown. For fatigue life predictions, a power law fit to the fully-reversed fatigue data was used as the prediction line, as expressed in Figs. 5a, 6a, 7a, 8a, and 9a.

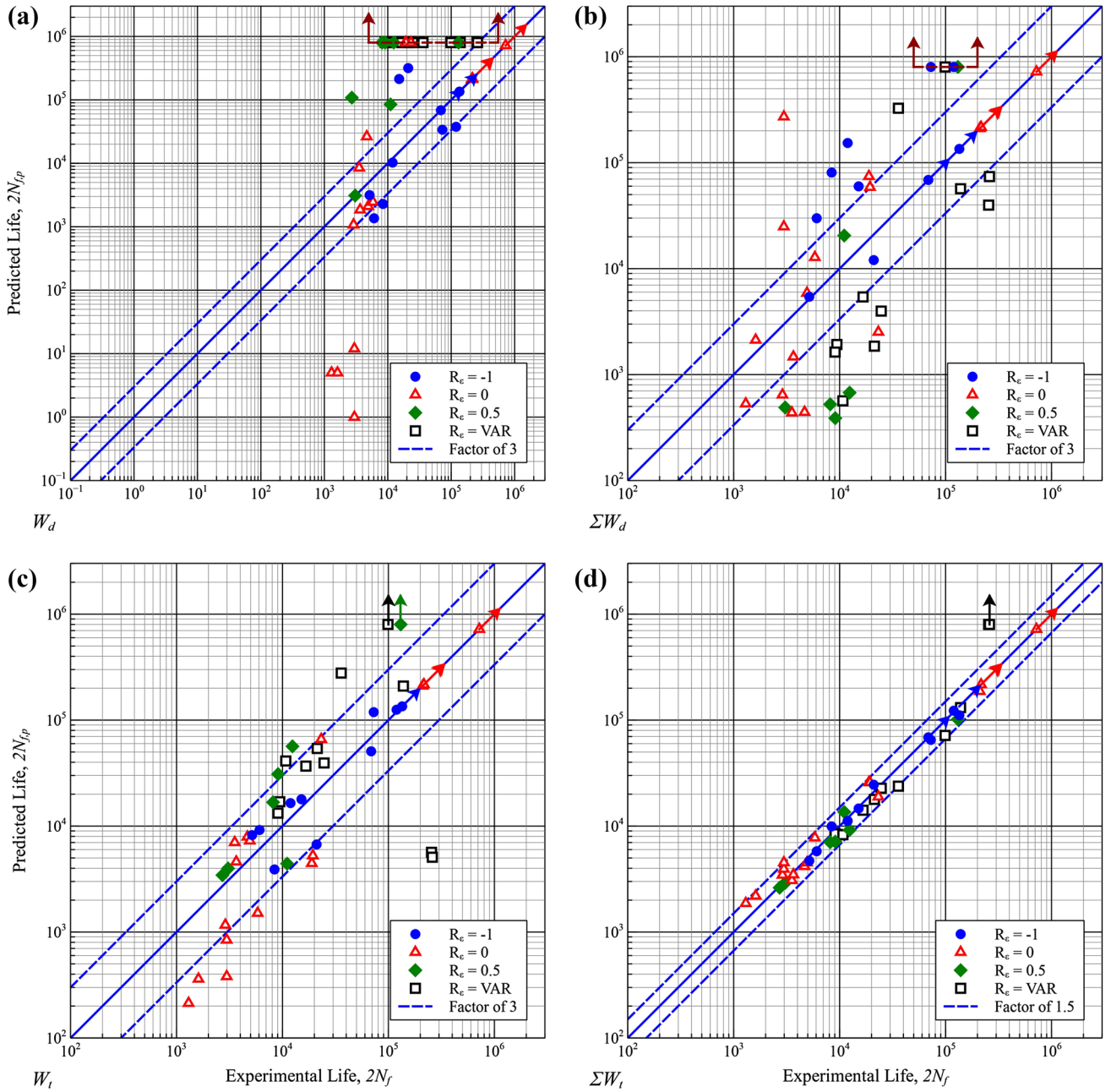

Fig. 10 Comparison of the predicted and experimentally observed fatigue lives for specimens with different transformation stresses under different strain ratios using various energy-based damage parameters: **a** W_d, **b** ΣW_d, **c** W_t, and **d** ΣW_t

As seen in Fig. 10a, most of the predictions based on the dissipated strain-energy-density, W_d, do not even fall within prediction bands of three for materials with different transformation stresses. The dissipated strain-energy-density parameter underestimates the fatigue damage for many tests specifically at larger strain ratios, and therefore, very long fatigue lives have been predicted for these specimens. Moreover, there are two main deficiencies in using this parameter for fatigue life analysis of superelastic NiTi. First, the model does not predict any damage for tests conducted in the linear elastic region, which is in contrast to what is reported in the literature [11–13] based on the experimental observations for superelastic NiTi.

Another disadvantage of the dissipated strain-energy-density damage parameter is in explaining the fatigue behavior under fully reversed loading at higher strains. According to the experimental results from the rotating bending fatigue testing, fatigue lives for specimens with a maximum stress on the stress plateau ($\varepsilon_s^{AM} \leq \varepsilon_{max} \leq \varepsilon_f^{AM}$) appear to be very similar [12]. However, the amount of dissipated strain-energy-density significantly increases with an increase in strain amplitude within the aforementioned range. While an increase in the dissipated strain-energy-density indicates a reduction in the fatigue life, this is not the case for superelastic NiTi as the fatigue lives have been reported to be very similar for this range of strain amplitudes in fully-reversed condition.

Similarly, most fatigue life predictions using the cumulative dissipated strain-energy-density, ΣW_d, as shown in Fig. 10b, are unsatisfactory and fall outside of the prediction bands of three. On the other hand, the deficiency of the dissipated strain-energy-density, W_d, in predicting zero fatigue damage for linear elastic region is also applicable to the cumulative dissipated strain-energy-density as a fatigue damage parameter.

Figure 10c compares the predicted fatigue lives based on the total strain-energy-density damage parameter, W_t, with the experimentally observed fatigue lives. As seen in this figure, although better fatigue life predictions are obtained using W_t parameter compared with the dissipated (Fig. 10a) and cumulative dissipated (Fig. 10b) strain-energy-density parameters, many data points are still outside of the prediction bands of three. The inaccurate fatigue life predictions using the total strain-energy-density model may be attributed not only to the different transformation stresses of NiTi specimens considered in this study, but also to the differences in the loading and unloading plateaus. Since this model, in its current form, is sensitive to the level of the transformation stress of the material, it works well for a set of data exhibiting comparable loading and unloading transformation stresses as can be noticed in Fig. 8b, and also reported in [20]. It is worth mentioning that, contrary to the dissipated strain-energy-density, W_d, the total strain-energy-density parameter, W_t, appropriately models the similar fatigue lives for the tests with large strain amplitudes under fully-reversed condition. This is mainly due to the significant contribution of the tensile austenitic strain-energy-density, W_e^+, to the overall damage parameter.

Figure 10d illustrates the capability of the proposed total fatigue toughness model, ΣW_t, for fatigue life prediction of superelastic NiTi with various transformation stresses, under different load ratios. As can be seen in this figure, majority of the predicted fatigue lives fall within prediction bands of 1.5. The proposed energy-based damage parameter considers the evolution in the cyclic response of the material, including the transient, initial behavior. Moreover, each term in the total energy density damage parameter (i.e., W_d and W_e^+) has its physical meaning and expresses the crack initiation and propagation stages of the material [23]. Gloanec and coworkers [38] reported that there would be a change in the hysteresis response of the superelastic NiTi upon formation of a microcrack. Subsequently, the variations in the stress–strain response will influence the fatigue behavior of the material, which can be only captured by a cumulative damage parameter.

One potential advantage of the energy-based fatigue damage parameters is the fact that they consider the effects of frequency (i.e., strain rate) on the fatigue behavior [36]. In general, for most materials, including superelastic NiTi, the test-frequency (i.e., strain rate) effects are reflected in the stress–strain response [28]. As a result, all the energy-based damage models that consider the shape of the hysteresis loop in calculating the fatigue damage implicitly account for the effects of test frequency. However, the main challenge with employing an energy-based damage parameter is the critical need for having reliable cyclic constitutive models. On the other hand, the energy-based damage models that simply calculate energy as a product of stress and strain, such as Smith–Watson–Topper parameter [39], may not accurately consider the frequency effect on the fatigue behavior.

As seen in Fig. 9, the total fatigue toughness (cumulative total strain-energy-density) against fatigue life data for all tests (specimens with different cyclic stress response under various strain ratios) follow a similar trend. This trend can be presented by a linear relationship between the total fatigue toughness and the fatigue life in the log–log scale. Thus, a set of fatigue tests (fully-reversed or with mean strain) on superelastic NiTi specimens (regardless of cyclic deformation response) that covers an appropriate range of fatigue lives can be used to determine the slope and intercept of the prediction line, assuming that the prediction line is a simple

power law equation (or a linear equation in log–log scale). For the sake of convenience, this set of tests can be selected such that it has fewer associated experimental challenges. For example, pulsating tension tests at different strain amplitudes can be appropriate for this purpose to avoid buckling of specimens.

Conclusions

Strain-controlled fatigue experiments from authors' previous works were used together with a new set of fatigue data on superelastic NiTi specimens with different cyclic deformation responses. The employed cyclic fatigue tests were at different conditions, including fully reversed (i.e., $R_\varepsilon = -1$) and with mean strains (i.e., $R_\varepsilon = 0$, 0.33, 0.5, 0.67, 0.9). A cumulative energy-based damage parameter—i.e., total fatigue toughness, $\sum W_t$—was proposed and evaluated for fatigue life analysis of superelastic NiTi. Based on the experimental observations and analysis results, the following conclusions can be made:

1. A proposed fatigue damage parameter based on the cumulative total strain-energy-density provides satisfactory correlations of fatigue data from superelastic NiTi specimens with different cyclic deformation responses and under various mean strain/stress loading (i.e., loading ratios).
2. While fatigue failures are reported for superelastic NiTi in the linear elastic region, a fatigue damage parameter based on only dissipated strain-energy-density does not consider any fatigue damage when deformation is fully elastic. Moreover, such a damage parameter cannot explain the similar fatigue lives observed for fully-reversed tests with a maximum strain on the stress plateau ($\varepsilon_s^{AM} \leq \varepsilon_{max} \leq \varepsilon_f^{AM}$).
3. The fatigue damage parameter based on the total strain-energy-density, W_t, considering both dissipated and austenitic strain-energies, while providing acceptable fatigue life predictions under various load ratios, its capability is limited to specimens with comparable stress–strain response (i.e., cyclic deformation response).
4. Fatigue damage parameters based on cumulative strain-energy-densities are capable of considering the transient behavior and evolution in deformation response of the material under cyclic loading.
5. As the strain-rate effects are typically reflected in the cyclic stress–strain response of the material, energy-based damage parameters that consider the shape of the hysteresis loop, such as those studied in this work, will implicitly account for the strain-rate effects on the fatigue behavior.

Acknowledgements Nima Shamsaei's contributions were partially supported by the National Science Foundation under Grant No. 1660446. Experiments were performed at the Center for Advanced Vehicular Systems at the Mississippi State University.

References

1. Petrini L, Wu W, Dordoni E, Meoli A, Migliavacca F, Pennati G (2012) Fatigue behavior characterization of Nitinol for peripheral stents. Funct Mater Lett 05:1250012. doi:10.1142/S1793604712500129
2. Johnson R, Padgett JE, Maragakis ME, DesRoches R, Saiidi MS (2008) Large scale testing of nitinol shape memory alloy devices for retrofitting of bridges. Smart Mater Struct 17:035018. doi:10.1088/0964-1726/17/3/035018
3. Amerinatanzi A, Moghaddam NS, Ibrahim H, Elahinia M (2016) Evaluating a NiTi implant under realistic loads: A simulation study. In: American Society of Mechanical Engineers
4. Moghaddam NS, Andani MT, Amerinatanzi A, Haberland C, Huff S, Miller M, Elahinia M, Dean D (2016) Metals for bone implants: safety, design, and efficacy. Biomanufacturing Rev 1:1. doi:10.1007/s40898-016-0001-2
5. Mohd Jani J, Leary M, Subic A, Gibson MA (2014) A review of shape memory alloy research, applications and opportunities. Mater Des 56:1078–1113
6. Mahtabi MJ, Shamsaei N, Mitchell MR (2015) Fatigue of Nitinol: The state-of-the-art and ongoing challenges. J Mech Behav Biomed Mater 50:228–254. doi:10.1016/j.jmbbm.2015.06.010
7. Mahtabi MJ, Shamsaei N, Elahinia MH (2015) Fatigue of shape memory alloys. In: Elahinia MH (ed) Shape memory alloy actuators. John, New York, pp 155–190
8. Robertson SW, Pelton AR, Ritchie RO (2012) Mechanical fatigue and fracture of Nitinol. Int Mater Rev 57:1–37
9. Runciman A, Xu D, Pelton AR, Ritchie RO (2011) An equivalent strain/Coffin–Manson approach to multiaxial fatigue and life prediction in superelastic Nitinol medical devices. Biomaterials 32:4987–4993. doi:10.1016/j.biomaterials.2011.03.057
10. Maletta C, Sgambitterra E, Furgiuele F, Casati R, Tuissi A (2012) Fatigue of pseudoelastic NiTi within the stress-induced transformation regime: a modified Coffin–Manson approach. Smart Mater Struct 21:112001. doi:10.1088/0964-1726/21/11/112001
11. Kim YS, Miyazaki S (1997) Fatigue properties of Ti-50.9 at% Ni shape memory wires. In: Pelton AR, Hodgson D, Russell SM, Duerig T (ed) Proceedings of the 2nd international conference on shape memory and superelastic technologies (SMST); Pacific Grove, MIAS SMST-97, pp 473–477
12. Pelton AR, Fino-Decker J, Vien L, Bonsignore C, Saffari P, Launey M, Mitchell MR (2013) Rotary-bending fatigue characteristics of medical-grade Nitinol wire. J Mech Behav Biomed Mater 27:19–32
13. Tobushi H, Hachisuka T, Yamada S, Lin P-H (1997) Rotating-bending fatigue of a TiNi shape-memory alloy wire. Mech Mater 26:35–42. doi:10.1016/S0167-6636(97)00019-7
14. Mahtabi MJ, Shamsaei N, Rutherford B (2015) Mean strain effects on the fatigue behavior of superelastic Nitinol alloys: an experimental investigation. Procedia Eng 133:646–654. doi:10.1016/j.proeng.2015.12.645
15. Moumni Z, Herpen AV, Riberty P (2005) Fatigue analysis of shape memory alloys: energy approach. Smart Mater Struct 14:S287. doi:10.1088/0964-1726/14/5/017
16. Predki W, Klönne M, Knopik A (2006) Cyclic torsional loading of pseudoelastic NiTi shape memory alloys: damping and fatigue failure. Mater Sci Eng A 417:182–189. doi:10.1016/j.msea.2005.10.037

17. Jensen DM (2005) Biaxial fatigue behavior of NiTi shape memory alloy. Air Force Institute of Technology
18. Mahtabi MJ, Shamsaei N (2016) Multiaxial fatigue modeling for Nitinol shape memory alloys under in-phase loading. J Mech Behav Biomed Mater 55:236–249. doi:10.1016/j.jmbbm.2015.10.022
19. Pelton AR, Schroeder V, Mitchell MR, Gong X-Y, Barney M, Robertson SW (2008) Fatigue and durability of Nitinol stents. J Mech Behav Biomed Mater 1:153–164
20. Mahtabi MJ, Shamsaei N (2016) A modified energy-based approach for fatigue life prediction of superelastic NiTi in presence of tensile mean strain and stress. Int J Mech Sci 117:321–333. doi:10.1016/j.ijmecsci.2016.08.012
21. Kan Q, Kang G, Yan W, Dong Y, Yu C (2012) An energy-based fatigue failure model for super-elastic NiTi alloys under pure mechanical cyclic loading. In: Proceedings of SPIE—the international society for optical engineering
22. Ellyin F, Kujawski D (1993) A multiaxial fatigue criterion including mean-stress effect. In: ASTM special technical publication, vol 1191, pp 55–66
23. Golos K, Ellyin F (1988) A total strain energy density theory for cumulative fatigue damage. J Press Vessel Technol 110:36–41. doi:10.1115/1.3265565
24. Gall K, Tyber J, Brice V, Frick CP, Maier HJ, Morgan N (2005) Tensile deformation of NiTi wires. J Biomed Mater Res A 75A:810–823. doi:10.1002/jbm.a.30464
25. Bagheri A, Mahtabi MJ, Shamsaei N (2016) Fatigue behavior and cyclic deformation of additive manufactured NiTi, Submitted publication
26. Pelton AR, Dicello J, Miyazaki S (2000) Optimisation of processing and properties of medical grade Nitinol wire. Minim Invasive Ther Allied Technol 9:107–118
27. Saedi S, Turabi AS, Taheri Andani M, Haberland C, Karaca H, Elahinia M (2016) The influence of heat treatment on the thermomechanical response of Ni-rich NiTi alloys manufactured by selective laser melting. J Alloy Compd 677:204–210. doi:10.1016/j.jallcom.2016.03.161
28. Shaw JA, Kyriakides S (1995) Thermomechanical aspects of NiTi. J Mech Phys Solids 43:1243–1281. doi:10.1016/0022-5096(95)00024-D
29. Mohd Jani J, Leary M, Subic A (2016) Designing shape memory alloy linear actuators: A review. J Intell Mater Syst Struct. doi:10.1177/1045389X16679296
30. Frenzel J, George EP, Dlouhy A, Somsen C, Wagner MF-X, Eggeler G (2010) Influence of Ni on martensitic phase transformations in NiTi shape memory alloys. Acta Mater 58:3444–3458. doi:10.1016/j.actamat.2010.02.019
31. Otsuka K, Ren X (2005) Physical metallurgy of Ti–Ni-based shape memory alloys. Prog Mater Sci 50:511–678. doi:10.1016/j.pmatsci.2004.10.001
32. Halford GR (1966) The energy required for fatigue (plastic strain hysteresis energy required for fatigue in ferrous and nonferrous metals). J Mater 1:3–18
33. Morrow J (1965) Cyclic plastic strain energy and fatigue of metals. In: Lazan B (ed) Internal friction, damping, and cyclic plasticity. ASTM International, West Conshohocken, PA, pp 45–87. doi:10.1520/STP43764S
34. Nip KH, Gardner L, Davies CM, Elghazouli AY (2010) Extremely low cycle fatigue tests on structural carbon steel and stainless steel. J Constr Steel Res 66:96–110. doi:10.1016/j.jcsr.2009.08.004
35. Lefebvre D, Ellyin F (1984) Cyclic response and inelastic strain energy in low cycle fatigue. Int J Fatigue 6:9–15. doi:10.1016/0142-1123(84)90003-3
36. Shrestha R, Simsiriwong J, Shamsaei N, Moser RD (2016) Cyclic deformation and fatigue behavior of polyether ether ketone (PEEK). Int J Fatigue 82(3):411–427. doi:10.1016/j.ijfatigue.2015.08.022
37. Yang B, Liaw PK, Morrison M, Liu CT, Buchanan RA, Huang JY, Kuo RC, Huang JG, Fielden DE (2005) Temperature evolution during fatigue damage. Intermetallics 13:419–428. doi:10.1016/j.intermet.2004.07.032
38. Gloanec A-L, Cerracchio P, Reynier B, Van Herpen A, Riberty P (2010) Fatigue crack initiation and propagation of a TiNi shape memory alloy. Scr Mater 62:786–789. doi:10.1016/j.scriptamat.2010.02.001
39. Smith KN, Watson P, Topper TH (1970) A stress–strain parameter for the fatigue of metals. J Mater 5:767–778